communications materials

ARTICLE

https://doi.org/10.1038/s43246-023-00337-8 OPEN

Manipulating O3/P2 phase ratio in bi-phasic sodium layered oxides via ionic radius control

P. A. Maughan[1,2], A. B. Naden[1], J. T. S. Irvine[1,2] & A. R. Armstrong[1,2]✉

Bi-phasic O3/P2 sodium layered oxides have emerged as leading candidates for the commercialisation of next-generation sodium-ion batteries. However, beyond simply altering the sodium content, rational control of the O3/P2 ratio in these materials has proven particularly challenging despite being crucial for the realization of high-performance electrode materials. Here, using abundant elements, we manipulate the O3/P2 ratio using the average ionic radius of the transition metal layer and different synthesis conditions. These methods allow deterministic control over the O3/P2 ratio, even for constant Na contents. In addition, tuning the O3/P2 ratio yields high-performing materials with different performance characteristics, with a P2-rich material achieving high rate capabilities and excellent cycling stability (92% retention, 50 cycles), while an O3-rich material displayed an energy density up to 430 Wh kg $^{-1}$, (85%, 50 cycles). These insights will help guide the rational design of future high-performance materials for sodium-ion batteries.

[1] School of Chemistry, University of St Andrews, St Andrews, Fife KY16 9ST, UK. [2] The Faraday Institution, Quad One, Harwell Science and Innovation Campus, Didcot OX11 0RA, UK. ✉email: ara@st-andrews.ac.uk

Sodium-ion batteries (SIBs) are widely expected to become a key low-cost next-generation energy storage solution with likely applications for grid storage, data centres, and lower-performance electric vehicles. To enable the successful commercialization of SIBs, it is essential to develop high-performance positive electrode materials based on low cost, high abundance, and non-toxic elements, which determine the overall energy density of the battery[1–4].

Of the most commonly studied groups of potential positive electrode materials, layered sodium metal oxides have multiple advantageous properties such as high capacity, voltage, and tap densities, all of which are key to realizing high energy densities[5,6]. These materials typically crystallize into two common structures known as the O3 and P2 phases, following the classification devised by Delmas et al (Fig. 1a, b)[7]. In both structures, sodium layers alternate with transition metal (TM) layers. Different oxygen stacking sequences give rise to different Na environments, with ABBA oxygen stacking in the P2 phase forming prismatic (P) Na sites, while the ABCABC oxygen stacking in the O3 structure forms octahedral (O) Na sites. O3-type materials typically have high Na contents, which enables high capacities and energy densities, but suffer from poor cycling stabilities due to multiple phase transitions occurring during cycling[5]. In addition, the relatively small Na interlayer spacing and complex Na diffusion channels through interstitial sites results in low capacities at higher rates, further limiting overall performance. In contrast, P2 materials typically display superior cycling stability with fewer phase transitions and enhanced rate performance due to large Na diffusion channels with direct pathways between prismatic sites[5]. However, P2 materials crystallize with low Na contents resulting in low capacities in full cells.

Therefore, it is desirable to develop advanced electrode materials with the cycling characteristics of P2-type materials but the high Na content (and therefore energy density) of O3-type oxides. The use of bi-phasic materials, which combine both the P2 and O3 type phases into a single material, has attracted significant attention in recent years as a potential solution[6,8–14]. Here, the O3 part of the material provides high Na content, enabling high capacities, while the P2 part of the structure stabilizes the material during cycling and facilitates fast Na diffusion. However, to-date, there is limited understanding on the rational control of the O3/P2 phase ratio, beyond simply changing the Na content. Furthermore, many of the existing reports on O3/P2 bi-phasic materials focus on inducing O3 formation within low Na content materials in the P2 region (Na = 2/3), which does not solve the problem of low capacities in full cells[8–11].

Recently, Zhao et al introduced the concept of cationic potential ($\Phi cation$) as a predictor for the formation of O3 or P2 crystal structures and used this to design a high Na content P2 material (Na > 0.80), which would typically be expected to crystallize in the O3 phase[15]. They defined the cationic potential as shown in Eq. 1, where ΦTM is the weighted ionic potential of the ions in the TM layer, with contributions from the charge (ni) and radius (Ri) of each ion (i), weighted stoichiometrically (wi), as shown in Eq. 2, ΦNa and ΦO are the weighted ionic potential of Na and O, respectively, as defined by Eqs. 3 and 4, where x corresponds to the content in Na_xTMO_2, and R is the ionic radius, and n is the magnitude of the charge. This demonstrated that careful selection of the elements in the transition metal layer could significantly affect the crystal structure of sodium layered oxides and revealed the influence of properties such as charge and ionic radius of the ions in the material in determining the final crystal structure, rationalized by relative electrostatic repulsion between the TM layers.

$$\Phi cation = \frac{\Phi TM \Phi Na}{\Phi O} \quad (1)$$

$$\Phi TM = \sum \frac{wi.ni}{Ri} \quad (2)$$

$$\Phi Na = \frac{x(Na).n}{R(Na)} \quad (3)$$

$$\Phi O = \frac{x(O).n}{R(O)} \quad (4)$$

In this work, we expand and refine the application of the cationic potential to design bi-phasic O3/P2 hybrid materials and compare the use of ionic radius and cationic potential as predictors, which results in the introduction of a new predictor for bi-phasic materials, the radial potential. We reveal how simply changing the chemical composition of 10% of the transition metal layer can tune the O3/P2 ratio through a range of O3/P2 bi-phasic materials, even without changing the Na content. In addition, the role of synthesis method is also examined, and allows a further degree of control over the resulting O3/P2 ratio. These insights allow the development of protocols to enable the rational design of O3/P2 bi-phasic materials with tuneable O3/P2 content, independent of Na content. This is demonstrated through the development of several high-performing SIB electrode materials based on low cost, high abundance, and low toxicity elements, based on the series $Na_xMn_{0.4}Fe_{0.4}Ti_{0.1}M_{0.1}O_2$, where x = 0.72 or 0.75 and M = Mg, Cu or Al.

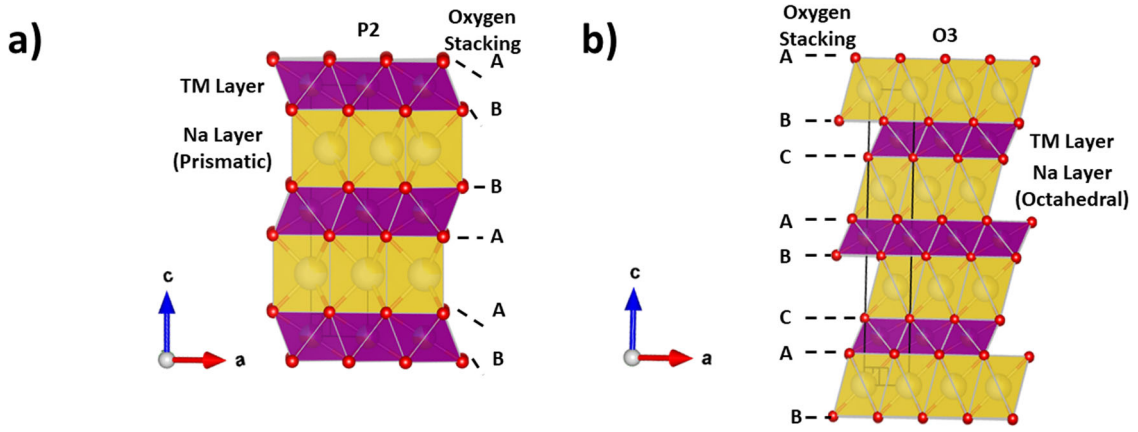

Fig. 1 Schematic diagram of typical P2 and O3 crystal structures that arise from different oxygen stackings, shown by the ABC labels. a Crystal structure of the P2 phase **b** Crystal structure of the O3 phase.

Table 1 Sol-gel synthesized materials with their sample designations, target chemical composition, and experimental chemical composition calculated from ICP.

Sample Name	Target chemical composition	Experimental chemical composition (ICP[a])	Phase Ratio (P2/O3)
Na72Ti1Al1	$Na_{0.72}Mn_{0.4}Fe_{0.4}Ti_{0.1}Al_{0.1}O_2$	$Na_{0.72}Fe_{0.42}Mn_{0.40}Ti_{0.09}Al_{0.09}O_2$	100/0
Na72Ti1Mg1	$Na_{0.72}Mn_{0.4}Fe_{0.4}Ti_{0.1}Mg_{0.1}O_2$	$Na_{0.72}Fe_{0.42}Mn_{0.40}Ti_{0.10}Mg_{0.08}O_2$	86/14
Na72Ti1Cu1	$Na_{0.72}Mn_{0.4}Fe_{0.4}Ti_{0.1}Cu_{0.1}O_2$	$Na_{0.73}Fe_{0.40}Mn_{0.40}Ti_{0.09}Cu_{0.11}O_2$	83/17
Na75Ti1Al1	$Na_{0.75}Mn_{0.4}Fe_{0.4}Ti_{0.1}Al_{0.1}O_2$	$Na_{0.77}Fe_{0.43}Mn_{0.40}Ti_{0.10}Al_{0.07}O_2$	27/73
Na75Ti1Mg1	$Na_{0.75}Mn_{0.4}Fe_{0.4}Ti_{0.1}Mg_{0.1}O_2$	$Na_{0.76}Fe_{0.42}Mn_{0.40}Ti_{0.10}Mg_{0.08}O_2$	11/89
Na75Ti1Cu1	$Na_{0.75}Mn_{0.4}Fe_{0.4}Ti_{0.1}Cu_{0.1}O_2$	$Na_{0.76}Fe_{0.40}Mn_{0.39}Ti_{0.09}Cu_{0.11}O_2$[a]	0/100

[a]denotes calculation from EDS where ICP was not possible.

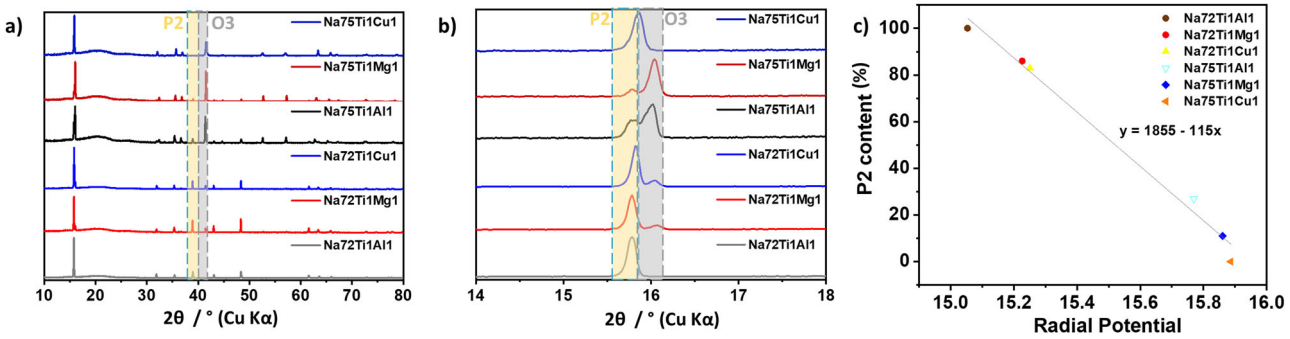

Fig. 2 Powder XRD patterns for sol-gel synthesised materials showing the change in P2:O3 ratio throughout the series. a Powder XRD patterns for the sol-gel synthesised series between 10–80 degrees. **b** Is an expansion of the data shown in **a**, highlighting the low angle (002) and (003) diffraction peaks, which correspond to the P2 and O3 structures respectively. **c** Plot of P2 content against radial potential, including a linear fit where $r^2 = 0.99$.

Results and discussion

Development of the radial potential. To investigate if the cationic potential approach could be expanded to help design O3/P2 bi-phasic sodium layered oxides, and to compare to the use of the average ionic radius of the transition metal layer elements as a predictor, a series of materials with the average composition $Na_xMn_{0.4}Fe_{0.4}Ti_{0.1}M_{0.1}O_2$, where $M = Mg^{2+}$, Zn^{2+}, Al^{3+} and $x = 0.72$ and 0.75, were synthesized using a simple sol-gel method. Powder X-ray diffraction (XRD) was used to determine the resulting crystal structure in each case. Rietveld refinements were carried out to calculate the O3/P2 ratio in each material, while inductively coupled plasma optical emission spectroscopy (ICP-OES) was used to confirm the elemental composition, results of which are listed in along with the sample designations in Table 1. Figure 2a, b show that only peaks relating to the P2 or O3 phase are present in each sample, ruling out the formation of other crystalline impurities. Strikingly, the obtained crystal structure varies significantly across the range of chemical compositions studied, with the material where Na72Ti1Al1 being revealed as a pure phase Na-rich P2 material, with no O3 peaks visible. In contrast, for Na75Ti1Cu1, only reflections corresponding to the O3 phase are present, revealing that the material is pure O3 phase. For all other compositions studied, reflections relating to both the P2 and O3 phases can be clearly observed, confirming successful synthesis of a range of O3/P2 bi-phasic materials, with differing P2 and O3 ratios. The individual refinement plots for each material, the refined lattice parameters along with the phase ratios can be found in the Supporting Information (Supplementary Fig. 1 and Supplementary Table 2, respectively).

The P2:O3 ratios for the sol-gel synthesised materials were 100:0 for Na72Ti1Al1, 86:14 for Na72Ti1Mg1, 83:17 for Na72Ti1Cu1, 27:73 for Na75Ti1Al1, 11:89 for Na75Ti1Mg1 and 0:100 for Na75Ti1Cu1, demonstrating the preparation of the entire range from fully P2 to fully O3, with a variety of different P2/O3 bi-phasic materials in between. As shown in Supplementary Fig. 2, the average TM ionic radius correlates well with a trend of increasing P2 content with decreased average radius within compositions of the same Na content (i.e., Na = 0.72 or 0.75), but cannot account well for the trend between different Na occupancies (Supplementary Fig. 2a). This implies that the Na content has a larger impact on the O3/P2 ratio than the size of the ions in the TM layer. Therefore, while ionic radius holds some promise as a predictor when the Na content is constant, it is not suitable when Na content is different in prospective materials. In contrast, the cationic potential cannot predict the trend for constant Na content, but accounts well for the effect of Na content significantly better than the average ionic radius (Supplementary Fig. 2b). Therefore, we propose an adapted predictor, the radial potential by combining the cationic potential and TM radius. Replacing the weighted transition metal potential, used in the calculation of the cationic potential, with the average ionic radius we define this radial potential as shown in Eq. 5:

$$RadialPotential = \frac{AverageTMradius * WeightedNapotential}{Weightedoxygenpotential} \quad (5)$$

As can be seen from Fig. 2c, there is a strong linear correlation between the P2 content and this radial potential across both Na ranges, where a smaller radial potential results in a higher P2 content. However, we note that while this can accurately predict materials synthesised in our group via one synthetic method e.g., sol-gel, it could not accurately predict some previously reported materials, some of which were predicted to be single phase when they were in fact bi-phasic. This is likely to be due to the different synthetic routes used and demonstrates the limits of this type of predictor. Nevertheless, we expect that for a given synthesis route, once a couple of data points are known, our method would then be useful in predicting the P2 content for future materials synthesised under the same conditions. It is also important to

Table 2 Solid-state synthesized materials with their sample names, target chemical composition, and actual chemical composition.

Sample Name	Target chemical composition	Experimental chemical composition (ICP)	Phase Ratio (P2/O3)
SS-Na75Ti1Mg1	$Na_{0.75}Mn_{0.4}Fe_{0.4}Ti_{0.1}Mg_{0.1}O_2$	$Na_{0.76}Fe_{0.43}Mn_{0.40}Ti_{0.10}Mg_{0.08}O_2$	6/94
SS-Na75Ti1Cu1	$Na_{0.75}Mn_{0.4}Fe_{0.4}Ti_{0.1}Cu_{0.1}O_2$	$Na_{0.76}Fe_{0.40}Mn_{0.41}Ti_{0.09}Cu_{0.11}O_2$	47/53
SS-Na75Ti1Zn1	$Na_{0.75}Mn_{0.4}Fe_{0.4}Ti_{0.1}Zn_{0.1}O_2$	$Na_{0.73}Fe_{0.41}Mn_{0.40}Ti_{0.09}Zn_{0.1}O_2$	7/93
SS-Na75Ti1Al1	$Na_{0.75}Mn_{0.4}Fe_{0.4}Ti_{0.1}Al_{0.1}O_2$	$Na_{0.75}Fe_{0.41}Mn_{0.40}Ti_{0.09}Al_{0.1}O_2$	82/18
SS-Na75Ti1Si1	$Na_{0.75}Mn_{0.4}Fe_{0.4}Ti_{0.1}Si_{0.1}O_2$	$Na_{0.82}Fe_{0.41}Mn_{0.43}Ti_{0.09}Si_{0.07}O_2$	100/0
SS-Mn5Fe5	$Na_{0.75}Mn_{0.5}Fe_{0.5}O_2$	$Na_{0.73}Fe_{0.51}Mn_{0.49}O_2$	55/45
SS-Ti1	$Na_{0.75}Mn_{0.5}Fe_{0.5}Ti_{0.1}O_2$	$Na_{0.74}Fe_{0.46}Mn_{0.45}Ti_{0.09}O_2$	53/47

note that the radial potential could accurately predict the trend of the P2 content with changing chemical composition (both Na and TM layer) for literature examples (Supplementary Table 3)[12].

To further investigate the effect of synthesis conditions, we also synthesised a family of materials with the overall composition $Na_{0.75}Mn_{0.4}Fe_{0.4}Ti_{0.1}M_{0.1}O_2$, where M = Mg^{2+}, Zn^{2+}, Al^{3+}, and Si^{4+} using a simple solid-state method. For comparison, the materials where M = 0 ($Na_{0.75}Mn_{0.45}Fe_{0.45}Ti_{0.1}O_2$) and both M and Ti = 0 ($Na_{0.75}Mn_{0.5}Fe_{0.5}O_2$) were also synthesized. The sample designations, chemical composition, and refined phase ratios are listed in Table 2. The use of the solid-state method enabled extra dopants, such as Si, to be used, the precursors of which are not cheaply available and easy to use for sol-gel synthesis, although the synthesised materials are typically less homogenous than the sol-gel synthesized materials (Supplementary Fig. 3). In this case, the P2:O3 ratios for Na75Ti1Si1 were 100:0, 82:18 for Na75Ti1Al1, 55:45 for the un-doped material $Na_{0.75}Mn_{0.5}Fe_{0.5}O_2$, 53:47 for $Na_{0.75}Mn_{0.45}Fe_{0.45}Ti_{0.1}O_2$ (M = 0), 47:53 for Na75Ti1Cu1, 7:93 for M = Na75Ti1Zn1 and 6:94 for Na75Ti1Mg1. The refinement plots for this series can be found in the Supporting Information, Supplementary Fig. 4 with the lattice parameters listed in Supplementary Table 4.

As was observed for the sol-gel synthesised series where the Na content was constant, the average ionic radius shows a better correlation with the P2 content than the cationic potential (Supplementary Fig. 5), with the radial potential predictor also demonstrating good correlation. However, the parameters required for the line of best fit are clearly different from the series synthesised by the sol-gel method, due to a significant shift towards higher P2 content in the solid-state synthesized materials (Supplementary Fig. 5d). Crucially, this demonstrates that choice of synthetic route is an additional important tool for the careful tuning of O3/P2 bi-phasic layered oxides. Clearly, simple chemical composition-based predictors cannot account for the effect of synthetic route, but can give guidance to aid the design of bi-phasic materials. This explains why the radial potential was unable to predict the O3/P2 ratio in literature materials accurately, where different synthesis conditions are used. In addition to synthesis route, synthesis conditions can also affect the phase ratio. For example, an increase in synthesis temperature increased the proportion of P2 content in Na72Ti1Cu1 from 78% to 84% when the calcination temperature was increased from 900 °C to 1000 °C (Supplementary Fig. 6).

We note that when the full analysis proposed by Zhao et al is carried out, and sodium ionic potential is plotted as a function of cationic potential, our compositions sit on their suggested dividing line between the P2 and O3 regions (Supplementary Fig. 7). Therefore, the cationic potential analysis can be used to determine whether a suggested composition is likely to fall within a bi-phasic region in the O3/P2 phase space, while the radial potential should then be used to determine if smaller compositional changes will increase or decrease the P2 (or O3) content. This combination of predictors enables the rational design and tuning of bi-phasic O3/P2 materials with variable phase ratios, potentially without changing the Na content.

Whilst there was generally a good correlation between the radial potential and the P2 content, this was not the case when M = Mg or Zn. Both these materials displayed higher O3 content than would be predicted. (Scanning) transmission electron microscopy, (S)TEM, illustrates the coexistence of the P2 and O3 phases and the formation of a Zn-rich superlattice in the P2 phase, as shown and described further in Supplementary Fig. 8. The formation of a superlattice in the P2 regions based upon Zn ordering could explain the increased O3 content in these materials, since this would change the relative stabilities of the two phases. Additionally, the stoichiometry will not be homogenous across the two phases, since the Zn ordering giving rise to the superlattice requires a higher Zn content than was in the target composition, which would result in a higher Zn content in the P2 phase and lower in the O3 phase. These differences can explain the higher-than-predicted O3 content in the Zn and Mg-containing materials.

Overall, the following guidelines should enable the successful rational design of O3/P2 bi-phasic materials with controlled O3/P2 ratios:

1. Use the cationic potential predictor to determine compositions close to the divide between P2 and O3 single phases.
2. The radial potential can then be used to predict the effect of small changes to the Na and TM layer compositions to increase or decrease the P2 content as desired.
3. Once one or two initial compositions have been synthesised at a given calcination temperature, a simple linear fit of a plot of the P2 content against the radial potential should enable the approximate prediction of P2 content of future materials, so long as the synthesis route is not altered.
4. Choice of synthesis route, precursors, calcination time, and temperature can all be used to enable additional tuning of the O3/P2 ratio.

Electrochemical Performance in Na-ion Batteries. Finally, to demonstrate the technological importance of these design strategies, example bi-phasic materials with a majority P2 and majority O3 phase composition were tested electrochemically in half-cell configurations for sodium-ion batteries (Fig. 3). The sol-gel synthesised P2/O3 bi-phasic materials Na72Ti1Cu1, was chosen as the example for a majority P2 bi-phasic material, and Na75Ti1Al1, was used to demonstrate a majority O3 bi-phasic material. We note that due to the differences in P2/O3 ratio and phase properties, where P2 typically displays higher voltages than O3 type materials, and the differences in the TM composition, the optimum voltage windows were slightly different for the two materials. The majority P2 Na72Ti1Cu1 material shows excellent cycling stability with 92% capacity retention over 50 cycles in the potential window of 2.3-4.2 V (Fig. 3 a,c), with high discharge capacity of 114 mAh g^{-1} resulting in an energy density of 365 Wh kg^{-1} (based on the mass

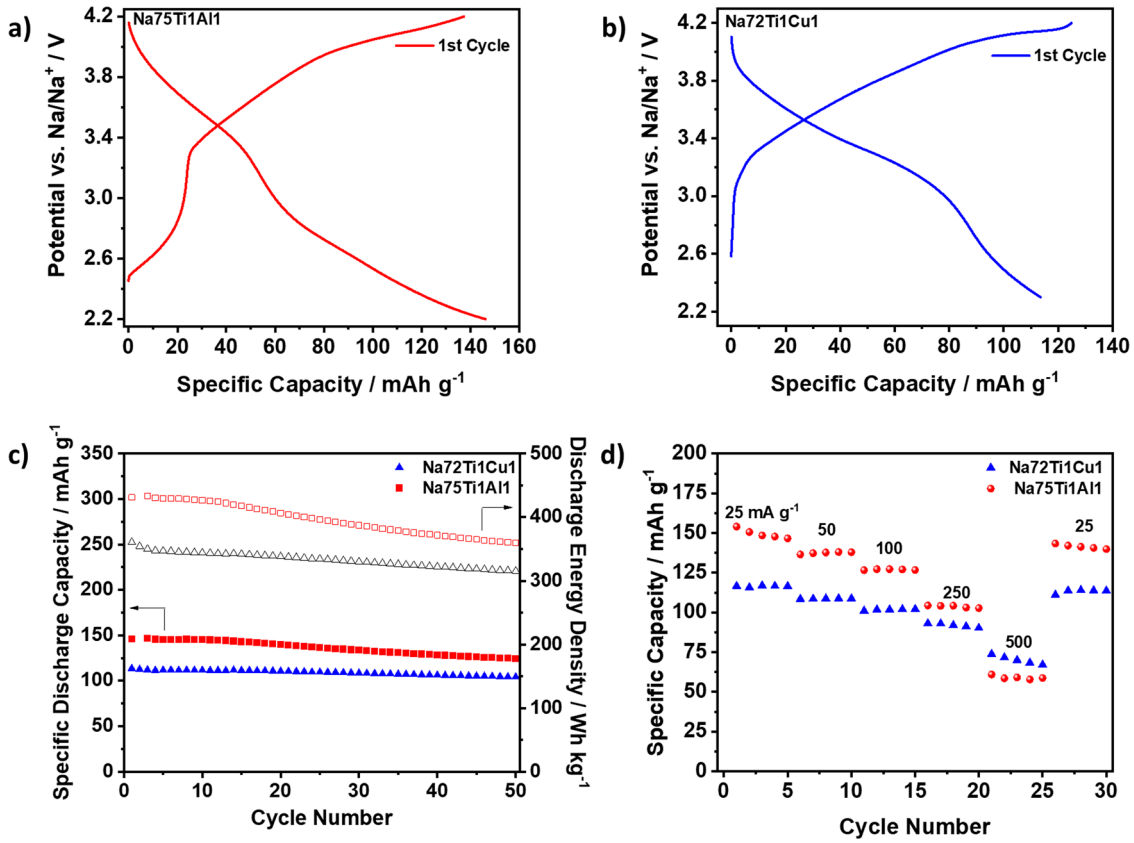

Fig. 3 Electrochemical performance of selected bi-phasic materials in Na-ion half cells. Voltage profile for the first cycle of **a** Na72Ti1Cu1 (2.3–4.2 V) and **b** Na75Ti1Al1 (2.2–4.2 V) cycled in a half cell against Na/Na^+ at a specific current of 25 mA g^{-1}. **c** Cycling stability showing the specific discharge capacities and discharge energy densities based on the mass of the active positive electrode material across 50 cycles. **d** Discharge capacities resulting from rate capability testing of Na72Ti1Cu1 and Na75Ti1Al1 at specific currents of 25, 50, 100, 250, and 500 mA g^{-1}.

of the active positive electrode). In addition, the material displayed excellent rate capability, retaining ca. 70 mAh g^{-1} even at the high rate of 500 mA g^{-1} (Fig. 3d).

The majority O3 bi-phasic material, Na75Ti1Al1, displayed a very high discharge capacity of 148 mAh g^{-1}, which resulted in an outstanding energy density of ca. 430 Wh kg^{-1}, which is among the highest known for nickel-free sodium layered oxides, and comparable to several Ni and/or Co containing Mn/Fe based materials (Fig. 4 and Supplementary Table 5)[16–28]. Even with such a high energy density, cycling stability was good with a capacity retention of 85% after 50 cycles. However, the rate capability was much poorer than observed for the majority P2 material, Na72Ti1Cu1, with only 59 mAh g^{-1} (40% of capacity at 25 mA g^{-1}) retained at 500 mA g^{-1} (Fig. 3d).

These results demonstrate that our approach can enable the design of high-performing electrode materials for Na-ion batteries, which can overcome the traditional disadvantages of the individual phases. Furthermore, by tuning the P2/O3 ratio, the performance characteristics of the resulting material can also be tuned and matched to desired applications. For example, using a majority P2 phase material such as Na72Ti1Cu1 can enable high power capabilities and long cycling lifetimes, while targeting an O3-rich bi-phasic material such as Na75Ti1Al1 can allow for very high reversible energy densities to be achieved, which would suit high energy but low power applications.

Conclusion

In conclusion, we have expanded the cationic potential predictor, recently developed to aid in the design of high Na P2 sodium layered oxides, to include predictions for the effect of changes in the chemical composition on the O3/P2 ratio in bi-phasic materials. This has led us to propose an adapted predictor, the radial potential, to complement the cationic potential, by focusing on using the average ionic radius of the TM layer to predict the effect of compositional changes on the O3/P2 ratio. This significantly improved the accuracy of predictions. It was also shown that synthesis methods and conditions can have a significant impact on the resulting phase ratios, which means that the radial potential predictor is best used when two or more data points are already known for the proposed compositional area. Overall, we proposed a strategy of combining the cationic potential and radial potential with careful control of the synthesis conditions to design high-performing Na-rich O3/P2 bi-phasic sodium layered oxides. This was demonstrated by the design and electrochemical testing of a P2-rich (Na72Ti1Cu1) and O3-rich (Na75Ti1Al1) O3/P2 biphasic materials. The P2-rich material showed excellent rate performance and outstanding cycling stability combined with high energy density (374 Wh kg^{-1}), while the O3-rich material displayed outstanding energy density of ca. 430 Wh kg^{-1}, which is among the highest reported for Ni-free sodium layered oxides and comparable to many Ni materials. These results showed how careful control of the P2/O3 ratio facilitated by the rational design strategy we proposed can yield high-performing electrode materials with properties that can be tuned to the desired application.

Experimental methods

Synthesis. Two different synthesis methods were used, sol-gel and solid-state. This allowed the effect of different synthesis methods on the resulting O3/P2 ratio to be studied. In addition, the use of the solid-state method enabled extra dopants, such as Si, to be

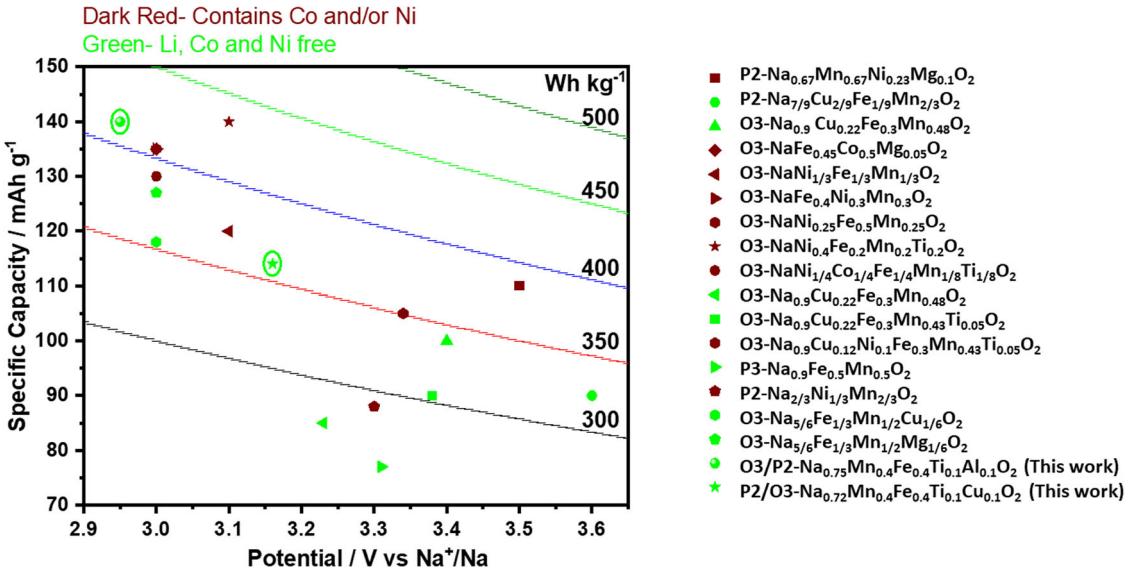

Fig. 4 Comparison of the first cycle discharge energy of various Mn/Fe-based sodium layered oxides. Selected materials contained sufficient Na for reasonable initial coulombic efficiencies, had a high average discharge potential of ca. 3 V or above and good cycling stability of at least 80% retention over at least 50 cycles. Dark red symbols correspond to Ni and/or Co-containing materials, while green symbols demonstrate that a material is Li, Co, and Ni-free. Our example bi-phasic materials are highlighted by green circles[16–28].

employed, the precursors of which are not cheaply available and easy to use in sol-gel synthesis.

Sol-gel synthesis. Materials in the series $Na_xMn_{0.4}Fe_{0.4}Ti_{0.1}M_{0.1}O_2$, where x = 0.72 or 0.75 and M = Mg, Cu, or Al, were synthesised using a citric acid sol-gel method. Stoichiometric amounts of sodium nitrate, manganese nitrate, iron nitrate, and either aluminium nitrate, magnesium nitrate, or copper nitrate were dissolved in de-ionized (DI) water and stirred for 10 mins, with a 2 wt.% excess of sodium nitrate. A stoichiometric quantity of TiO_2 nanopowder was then added to the solution under stirring, and left to homogenize under stirring for a further 10 mins. Citric acid was dissolved in a separate beaker (using a 1:1 citric acid to metal molar ratio) before addition to the nitrate solution. After stirring for 2 h, ammonium nitrate solution was added to control the pH from 1 to 8. The solution was then left to stir for a further 2 h, before heating to 80 °C overnight for gel formation. The gel was then dried at 130 °C for 6 h, before being ground in a pestle and mortar and calcined under air for 4 h at 500 °C, followed by 12 h at 900 °C using a heating/cooling rate of 5 °C/min. Once cooled to 250 °C, the samples were removed and ground in a dry room before transferring to an argon-filled glovebox.

Solid-state synthesis. Materials in the series $Na_{0.75}Mn_{0.4}Fe_{0.4}Ti_{0.1}M_{0.1}O_2$, where M = Mg, Zn, Cu, Al, Si, and where no M = 0 ($Na_{0.75}Mn_{0.45}Fe_{0.45}Ti_{0.1}O_2$) and no M and Ti = 0 ($Na_{0.75}Mn_{0.5}Fe_{0.5}O_2$) were used, were synthesized using a solid-state method. Stoichiometric amounts of sodium carbonate (with a 2% wt. excess), Mn_3O_4, Fe_2O_3, TiO_2, MgO, ZnO, Cu_2O, Al_2O_3, and SiO_2 were ball milled for 1 h (400 rpm), pelletized, and calcined under air for 12 h at 900 °C using a heating/cooling rate of 5 °C/min. Once cooled to 250 °C, the samples were removed and ground in a dry room before transferring to an argon-filled glovebox.

Material characterization. Powder x-ray diffraction (XRD) patterns were collected recorded on a PANalytical Empyrean diffractometer in Bragg-Brentano geometry with Cu $K\alpha_1$ radiation ($\lambda = 1.5406$ Å). Structures were refined by the Rietveld method using Topas Academic V6[29]. Scanning electron microscopy (SEM) images of as-synthesized materials coupled with Energy Dispersive x-ray spectroscopy (EDS) were recorded on a JEOL JSM-6700F.

(Scanning) transmission electron microscopy, (S)TEM, was performed on probe-corrected FEI Titan Themis operated at 200 kV and equipped with a CETA CCD camera and Fischionne M3000 high angle annular dark field (HAADF) detector. HAADF images were collected with a probe convergence angle of 21.2 mrad and inner/outer collection angles of 36.2 and 200 mrad, respectively.

Electrochemical characterization. To investigate the electrochemical performance of the materials, slurries were prepared using the active material super C65 carbon and Solef 5130 binder (a modified polyvinylidene fluoride (PVDF)) in the mass ratio 80: 10: 10 in n-methyl-2-pyrrolidone (NMP), which was cast onto aluminum foil using a doctor blade. After drying, 13 mm diameter electrode discs were punched and used to prepare CR2325 coin cells. All slurry processing, casting, drying, punching, and coin cell assembly was carried out in an argon-filled glovebox ($O_2 < 0.1$ ppm, $H_2O < 0.1$ ppm.). Sodium metal was used as a counter/reference electrode, a glass fiber paper (Whatman, GF/F) was used as the separator, and 1 M $NaPF_6$ in ethylene carbonate/diethyl carbonate (1:1 v/v%), Kishida as the electrolyte. Galvanostatic charge/discharge cycling and cyclic voltammetry were carried out at 30 °C using a Biologic BCS-805 battery cycler.

Predictor calculations. For the calculation of the values for the average transition metal layer ionic radius, cationic potential and radial potential, the standard values for ionic radius and charge were used for the respective ions, as used in the work by Zhao et al[15]. All ions had a fixed charge, apart from Mn, which could form either Mn^{3+} or Mn^{4+}, depending on the requirement for charge neutrality for the synthesised materials. The values used for each ion are listed in Supplementary Table 1.

Data availability

Data is available from the corresponding author upon request.

Received: 17 October 2022; Accepted: 23 January 2023;
Published online: 02 February 2023

References

1. Vaalma, C., Buchholz, D., Weil, M. & Passerini, S. A cost and resource analysis of sodium-ion batteries. *Nat. Rev. Mater.* **13**, 1–11 (2018).
2. Hwang, J. Y., Myung, S. T. & Sun, Y. K. Sodium-ion batteries: present and future. *Chem. Soc. Rev.* **21**, 3529–3614 (2017).
3. Deng, J. et al. Sodium-ion batteries: from academic research to practical commercialization. *Adv. Energy Mater.* **5**, 1701428 (2018).
4. Chen, M. et al. High-abundance and low-cost metal-based cathode materials for sodium-ion batteries: problems, progress, and key technologies. *Adv. Energy Mater.* **11**, 1803609 (2019).
5. Han, M. H., Gonzalo, E., Singh, G. & Rojo, T. A comprehensive review of sodium layered oxides: powerful cathodes for Na-Ion batteries. *Energy. Environ. Sci.* **1**, 81–102 (2015).
6. Rudola, A. et al. Commercialisation of high energy density sodium-ion batteries: Faradion's journey and outlook. *J. Mater. Chem. A* **7**, 8279–8302 (2021).
7. Delmas, C., Fouassier, C. & Hagenmuller, P. Structural classification and properties of the layered oxides. *Physica B+C* **99**, 81–85 (1980).
8. Lee, E. et al. Layered P2/O3 intergrowth cathode: toward high power Na-Ion batteries. *Adv. Energy Mater.* **4**, 1400458 (**2014**).
9. Guo, S. et al. A layered P2- and O3-type composite as a high-energy cathode for rechargeable sodium-ion batteries. *Angew. Chemie - Int. Ed.* **54**, 5894–5899 (2015).
10. Bianchini, M. et al. Layered P2-O3 sodium-ion cathodes derived from earth-abundant elements. *J. Mater. Chem. A* **6**, 3552–3559 (2018).
11. Li, Z. Y. et al. Li-substituted Co-free layered P2/O3 Biphasic $Na_{0.67}Mn_{0.55}Ni_{0.25}Ti_{0.2}$-$XLixO_2$ as high-rate-capability cathode materials for sodium ion batteries. *J. Phys. Chem. C* **120**, 9007–9016 (2016).
12. Qi, X. et al. Design and comparative study of O3/P2 hybrid structures for room temperature sodium-ion batteries. *ACS Appl. Mater. Interfaces* **9**, 40215–40223 (2017).
13. Zhou, D., Huang, W., Lv, X. & Zhao, F. A novel P2/O3 Biphase $Na_{0.67}Fe_{0.425}Mn_{0.425}Mg_{0.15}O_2$ as cathode for high-performance sodium-ion batteries. *J. Power Sources* **421**, 147–155 (2019).
14. Yang, L. et al. A Co- and Ni-free P2/O3 Biphasic Lithium stabilized layered oxide for sodium-ion batteries and its cycling behavior. *Adv. Funct. Mater.* **30**, 2003364 (2020).
15. Zhao, C. et al. Rational design of layered oxide materials for sodium-ion batteries. *Science* **370**, 708–712 (2020).
16. Yoda, Y. et al. Elucidating influence of Mg- and Cu-doping on electrochemical properties of O3-Nax[Fe, Mn]O_2 for Na-Ion batteries. *Small* **16**, 2006483 (2020).
17. Zhao, C. et al. Revealing high Na-Content P2-type layered oxides as advanced sodium-ion cathodes. *J. Am. Chem. Soc.* **142**, 5742–5750 (2020).
18. Mu, L. et al. Prototype Sodium-ion batteries using an air-stable and Co/Ni-free O_3-layered metal oxide cathode. *Adv. Mater.* **27**, 6928–6933 (2015).
19. Li, Y. et al. Air-stable copper-based P2-Na7/9Cu_2/9Fe1/9Mn_2/3O_2 as a new positive electrode material for sodium-ion batteries. *Adv. Sci.* **2**, 1500031 (2015).
20. Wang, P. F. et al. Suppressing the P2–O2 phase transition of $Na_{0.67}Mn_{0.67}Ni_{0.33}O_2$ by magnesium substitution for improved sodium-ion batteries. *Angew. Chemie - Int. Ed.* **55**, 7445–7449 (2016).
21. Tripathi, A., Xi, S., Gajjela, S. R. & Balaya, P. Introducing Na-sufficient P3-$Na_{0.9}Fe_{0.5}$Mn0.5O_2 as a cathode material for Na-ion batteries. *Chem. Commun.* **56**, 10686–10689 (2020).
22. Tripathi, A., Rudola, A., Gajjela, S. R., Xi, S. & Balaya, P. Developing an O_3 type layered oxide cathode and its application in 18650 commercial type Na-ion batteries. *J. Mater. Chem. A* **7**, 25944–25960 (2019).
23. Yue, J. L. et al. A quinary layer transition metal oxide of NaNi1/4Co1/4Fe1/4Mn1/8Ti1/8O_2 as a high-rate-capability and long-cycle-life cathode material for rechargeable sodium-ion batteries. *Chem. Commun.* **51**, 15712–15715 (2015).
24. Sun, X. et al. Na[$Ni_{0.4}Fe_{0.2}Mn_{0.4}$-XTix]O_2: A cathode of high capacity and superior cyclability for Na-ion batteries. *J. Mater. Chem. A* **2**, 17268–17271 (2014).
25. Oh, S. M. et al. Advanced Na[$Ni_{0.25}Fe_{0.5}Mn_{0.25}$]O 2/C-$Fe_3O_4$ Sodium-ion batteries using EMS electrolyte for energy storage. *Nano Lett.* **14**, 1620–1626 (2014).
26. Yabuuchi, N., Yano, M., Yoshida, H., Kuze, S. & Komaba, S. Synthesis and electrode performance of O3-Type NaFeO 2 -NaNi 1/2 Mn 1/2 O 2 solid solution for rechargeable sodium batteries. *J. Electrochem. Soc.* **160**, A3131–A3137 (2013).
27. Kim, D. et al. Layered Na[Ni 1/3Fe 1/3Mn 1/3]O 2 cathodes for Na-Ion battery application. *Electrochem. Commun.* **18**, 66–69 (2012).
28. Yao, H. R. et al. Excellent comprehensive performance of Na-based layered oxide benefiting from the synergetic contributions of multimetal ions. *Adv. Energy Mater.* **7**, 1700189 (2017).
29. Coelho, A. A. TOPAS and TOPAS-academic: an optimization program integrating computer algebra and crystallographic objects written in C++. *urn:issn:1600-5767* **51**, 210–218 (2018).

Acknowledgements

This work was supported by the Faraday Institution (Grant number FIRG018). The authors would like to thank Dr. David Rochester at Lancaster University for conducting the ICP-OES experiments. A.B.N. would like to acknowledge funding by the Engineering and Physical Sciences Research Council under grant numbers EP/L017008/1, EP/R023751/1, and EP/T019298/1 for the electron microscopy analysis.

Author contributions

P.A.M. and A.R.A. conceived and designed this work; P.A.M. carried out the ionic radius calculations, materials synthesis, XRD, and electrochemical characterisation. ABN carried out the SEM, EDS, and STEM experiments and analysis. P.A.M., A.B.N., J.T.S.I., and A.R.A. participated in the discussions of the experimental data and preparation of the manuscript.

Competing interests

P.A.M. and A.R.A. declare the international patent "Layered sodium metal oxides for Na-ion batteries" PCT/GB2022/052656. All other authors declare no competing financial interest.

Additional information

Supplementary information The online version contains supplementary material available at https://doi.org/10.1038/s43246-023-00337-8.

Correspondence and requests for materials should be addressed to A. R. Armstrong.

Peer review information *Communications Materials* thanks the anonymous reviewers for their contribution to the peer review of this work. Primary Handling Editors: Jet-Sing Lee and John Plummer.

Reprints and permission information is available at http://www.nature.com/reprints

Publisher's note Springer Nature remains neutral with regard to jurisdictional claims in published maps and institutional affiliations.